SPIKE a Physical Optics based Code for the Analysis of Antenna Radome Interactions

Mr C. D. Finlay*, Dr Stuart Gregson , Dr R. W. Lyon***, Dr J. McCormick*****

*SELEX SAS, Edinburgh U.K, +44 131-343-5776 christopher.finlay@selex-sas.com
**Formerly of SELEXSAS Now at NSI Near Field Systems Inc sgregson@nearfield.com
***SELEX SAS, Edinburgh U.K, +44 131-343-5775 ronald.lyon@selex-sas.com
****SELEX SAS, Edinburgh U.K, +44 131-343-5774 john.mccormick2@selex-sas.com

Keywords: Antennas, Physical Optics, Radomes.

Abstract

This paper presents a new physical optics based radome code SPIKE which has been used by SELEX S&AS to assess the impact of radomes on antenna performance. After a brief summary of the mathematical basis of the code some advantages of Physical Optics such as the ability to predict 2nd flashlobes and calculate the near fields in the vicinity of the antenna are demonstrated. Finally a comparison of flight trials data with results obtained from SPIKE in conjunction with a radar detection model GARD is made.

1 Introduction

A traditional approach to modelling the effects of a given radome on the performance of a specific radar has been to use ray-tracing. For example [1] Whilst this method is perfectly adequate for general purposes it is usually limited to calculating the effects of the first flashlobe and transmission loss through the radome on the far field radiation pattern. More recently we have developed a physical optics program dubbed SPIKE (Simple Physical Integration of Kirchoff's Equations.). Some of the advantages of using SPIKE are as follows:

- In contrast to the ray-tracing approach, with the "physical optics" method there is no need to model each identified specific scattering mechanism explicitly; in SPIKE this is done by a process of iteration. In ray-tracing terms each iteration corresponds to the number of bounces of the radiation from the antenna off the radome wall. This gives rise to flashlobes which show up as increased side lobe levels in well defined regions in the radiation pattern. Ray-tracing usually only models the first bounce and is thus limited to the calculation of the principal flashlobe.
- ♦ SPIKE models the radome surface numerically. Moreover, multiple surfaces can be modelled. In contrast RAP could only model ogives
- ♦ A traditional objection to the implementation of physical optics has been the long run times. The advent of high-CPU-power PCs has nullified this objection.

2 Mathematical basis

SPIKE is based on the Kirchoff Huygens Principle which enables the fields on one surface to be propagated to another point. The form of the Huygens principle which is used in SPIKE can be derived from the integral form of the Stratton Chu equations [3]. In general the $\underline{E}$ fields at a point P from a given surface can be calculated from the fields on the surface as follows:

$$\underline{E}_p = \frac{1}{4\pi}\int_S \left[\begin{array}{l} -j\omega\mu\left(\underline{n}\times\underline{H}\right)+ \\ \left\{\left(\underline{n}\times\underline{E}\right)\times\hat{\underline{r}}' + \left(\underline{n}\cdot\underline{E}\right)\hat{\underline{r}}'\right\}\left(jk_0+\frac{1}{r'}\right)\end{array}\right]\frac{e^{-jk_0r'}}{r'}ds_0 \quad (1)$$

With a similar expression for the magnetic field $\underline{H}$

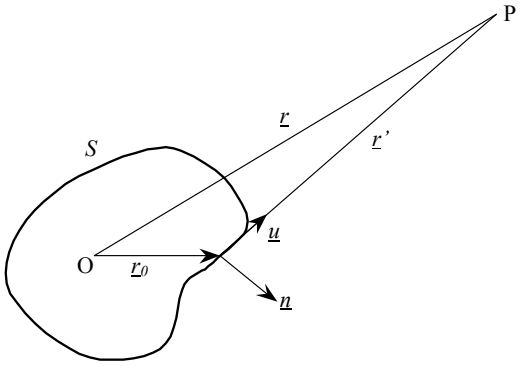

Figure 1 Geometry for equation 1.

Equation 1 is valid for both near field and far field calculations.

For a given antenna the **E** and **H** fields can be obtained by calculation or measurement. In the case of calculation a

simple method is the subaperture method. In this case the far fields of the antenna are given by

$$\underline{E}(r,\theta,\phi) = \sum_{n=1}^{N} a_n \underline{E}_n(\theta,\phi)\frac{e^{-jk0r_n}}{r_n} \qquad (2)$$

Where $\underline{E}_n$ is the element pattern of each subaperture, a_n are the amplitudes and r_n is the distance of the subaperture from the given point. The subaperture method can be used to calculate the illumination of the radome wall. Equation 2 is used to propagate the electromagnetic fields to the radome wall. In general for a given subaperture the fields are assumed to emanate from an infinitesimal point source at the centre of the subaperture, this means that it will radiate a spherical wave. However as the observation point on the inside of the radome is finitely far removed from the source it will be in the far field of the subaperture. Hence at the observation point the field will be of the form of a TEM plane wave propagating in the direction $\underline{r}$ '. As the field at the radome wall is a local plane wave the amount of field that is reflected and transmitted can be determined using the standard S matrix theory outlined below. The magnetic field resulting from the subaperture being obtained from the plane wave condition

$$d\underline{H}_{trans} = \frac{1}{Z_0}\hat{u}_i \times \underline{E}_{trans} ds \qquad (3)$$

Given the fields incident on the radome wall the transmitted and reflected fields are calculated as follows:

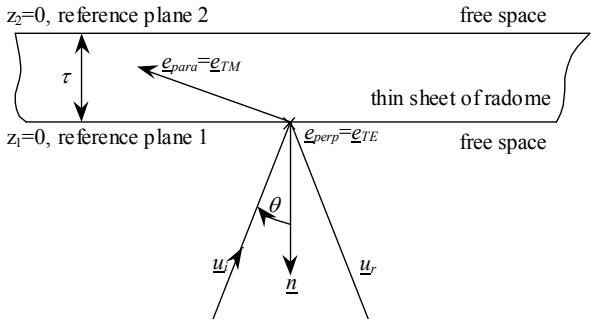

Figure 2: Calculation of transmitted and reflected fields on radome wall.

Define the parallel and perpendicular unit vectors

$$\hat{\underline{e}}_{TE} = \hat{\underline{e}}_{\perp} = \frac{\hat{\underline{n}} \times \hat{\underline{u}}_i}{\left|\hat{\underline{n}} \times \hat{\underline{u}}_i\right|} \qquad (4)$$

$$\hat{\underline{e}}_{TM} = \hat{\underline{e}}_{||} = \frac{\hat{\underline{u}}_i \times \hat{\underline{e}}_{\perp}}{\left|\hat{\underline{u}}_i \times \hat{\underline{e}}_{\perp}\right|} \qquad (5)$$

The transmitted electric field on the outer surface of the wall can be related to the incident electric fields as

$$\underline{E}_{trans} = S_{21TE}\left(\underline{E}_i \cdot \hat{\underline{e}}_{TE}\right)\hat{\underline{e}}_{TE} + S_{21TM}\left(\underline{E}_i \cdot \hat{\underline{e}}_{TM}\right)\hat{\underline{e}}_{TM} \qquad (6)$$

Where S_{21TE} , S_{21TM} are the scattering matrix elements of the radome wall which can be obtained either by calculation or measurement. Similarly the reflected fields are given by

$$\underline{E}_{reflec} = S_{11TE}\left(\underline{E}_i \cdot \hat{\underline{e}}_{TE}\right)\hat{\underline{e}}_{TE} + S_{11TM}\left(\underline{E}_i \cdot \hat{\underline{e}}_{TM}\right)\hat{\underline{e}}_{TM} \qquad (7)$$

Thus, the total transmitted electric field can be obtained by summing all of the contributions from the subapertures. Mathematically, this can be expressed as,

$$\underline{E}_{trans} = \int_S \begin{bmatrix} S_{21TE}\left(\underline{E}_i \cdot \hat{\underline{e}}_{TE}\right)\hat{\underline{e}}_{TE} + \\ S_{21TM}\left(\underline{E}_i \cdot \hat{\underline{e}}_{TM}\right)\hat{\underline{e}}_{TM} \end{bmatrix} ds \qquad (8)$$

$$\underline{H}_{trans} = \frac{1}{Z_0}\int_S \hat{\underline{u}}_i \times \begin{bmatrix} S_{21TE}\left(\underline{E}_i \cdot \hat{\underline{e}}_{TE}\right)\hat{\underline{e}}_{TE} \\ + S_{21TM}\left(\underline{E}_i \cdot \hat{\underline{e}}_{TM}\right)\hat{\underline{e}}_{TM} \end{bmatrix} ds \qquad (9)$$

Conversely, the reflected electric field can be obtained from,

$$\underline{E}_{reflec} = \int_S \begin{bmatrix} S_{11TE}\left(\underline{E}_i \cdot \hat{\underline{e}}_{TE}\right)\hat{\underline{e}}_{TE} + \\ S_{11TM}\left(\underline{E}_i \cdot \hat{\underline{e}}_{TM}\right)\hat{\underline{e}}_{TM} \end{bmatrix} ds \qquad (10)$$

As the reflected field will also be locally planar, the reflected magnetic field can be determined from,

$$\underline{H}_{reflec} = \frac{1}{Z_0}\int_S \hat{\underline{u}}_r \times \begin{bmatrix} S_{11TE}\left(\underline{E}_i \cdot \hat{\underline{e}}_{TE}\right)\hat{\underline{e}}_{TE} + \\ S_{11TM}\left(\underline{E}_i \cdot \hat{\underline{e}}_{TM}\right)\hat{\underline{e}}_{TM} \end{bmatrix} ds \qquad (11)$$

Within this analysis it is assumed that the semi-infinite slab of radome wall is tangential to the radome surface at each of the observation points.

The above equations will account for the direct transmitted and reflected fields. However in order to account for second order effects such as flashlobes it is necessary to include the contribution of the fields of the elements of the inner radome surface as part of the initial surface . This method is called 2nd order physical optics.

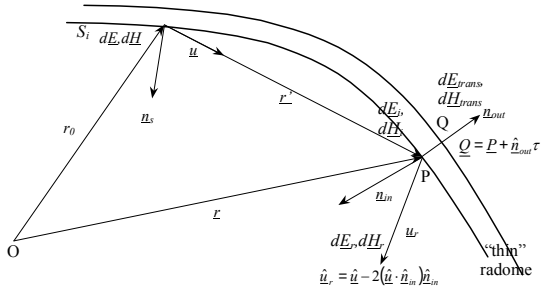

Figure 3: 2nd order contributions.

This process can in principle be repeated as many times as desired each iteration corresponding to a reflection off the radome wall. The total electric field on the radome wall surface can thus be represented as

$$\underline{E} = \underline{E}_{direct} + \underline{E}_{firstbounce} + \underline{E}_{secondbounce} + \underline{E}_{thirdbounce} + \cdots \quad (12)$$

Main flashlobes will appear from the contribution of the first bounce, 2nd flashlobes will appear from the contribution of the second bounce and so forth.

Finally the far field patterns are obtained from the far field approximation to the Kirchoff Huygen's principle [3]

$$\underline{E}_p = \frac{e^{-jk_0 r}}{k_0 r} \frac{\pi}{j\lambda^2} \int_S \left[\hat{r} \times (\underline{n} \times \underline{E}) + Z\hat{r} \times \{(\underline{n} \times \underline{H}) \times \hat{r}\} \right] e^{jk_0 \hat{r} \cdot \underline{r}_0} \, ds_0 \quad (13)$$

The magnetic fields if desired being obtained by the plane wave condition as before. Structure such as lightning strips and blockage can be modelled to first order by treating the appropriate part of the radome either as a totally reflecting surface or as a perfect absorbing surface.

3 Far Field Patterns showing 2nd Flashlobes

This section demonstrates the use of SPIKE to obtain far field radiation patterns for a typical radome antenna configuration.. The radome was an ogive of height 3 m and radius 600 mm (figure 9). The wall construction was chosen to have the same dielectric properties of an epoxy/E glass composite and was of constant thickness of 7.5 mm. The antenna was a circular antenna of diameter 900mm subdivided into 1280 subapertures of size 22.5*22.5 mm. The far field pattern of each subaperture being a sinc function (the code also includes alternative element pattern options to model the performance of electronically scanned array antennas). The radiation pattern was that of a circular Taylor distribution with Nbar set equal to 1 and Side Lobe level = -30.0 dB.. The antenna is mechanically scanned with vertical polarisation.

Figure 4 shows the free space far field radiation pattern of the antenna. Figure 5 shows the far field radiation pattern of the antenna with the beam pointing through the nose for 2 iterations. The main rings close to the main beam correspond to the first flashlobe region. The second flashlobe region is clearly discernable as a set of fainter second rings. Thus SPIKE is able to account for more features than a conventional ray tracing approach.

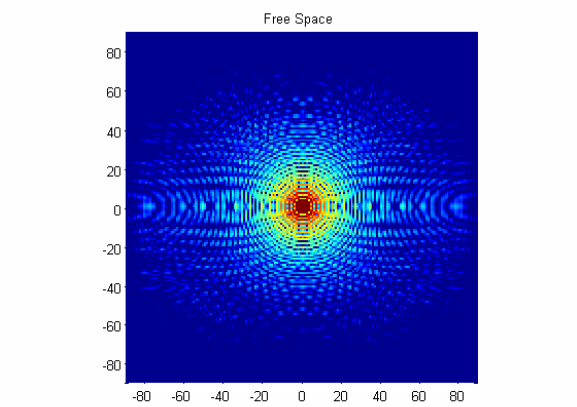

Figure 4: Free Space Far Field radiation pattern.

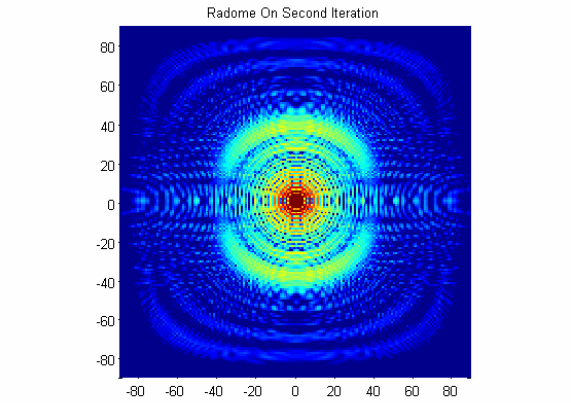

Figure 5: 2nd iteration showing presence of first and second flashlobes.

4 Near Field Predictions

Recently SPIKE has been used to calculate the near field of the antenna in various circumstances. One particular application was to calculate the on axis near field of an aperture antenna in free space. The near fields were calculated using the subaperture method and propagated to a plane surface orthogonal to the antenna. The resulting pattern is shown in figure 6 below. It shows an increase in the on axis field strength of upto 3 dB's.

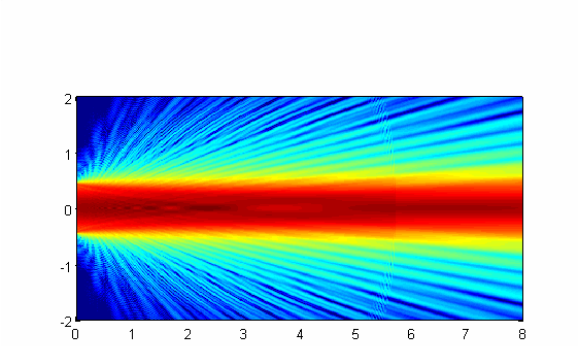

Figure 6: On axis near field of a typical antenna

Whilst this increase is at first sight somewhat surprising it corresponds to the optical phenomenon known as Poisson's spot [2]. It is encouraging that SPIKE is able to capture the essential features of this phenomenon.

One application of interest is the calculation of the magnitude of the E field in the region of the cockpit. A typical plot is shown in figure 7. The main beam points upwards and the principal flashlobe points downwards these are modelled reasonably accurately however the back diffraction at the interface between the cockpit and the edge of the radome is only indicative of the real situation due to the artificial cut off between radome and cockpit.

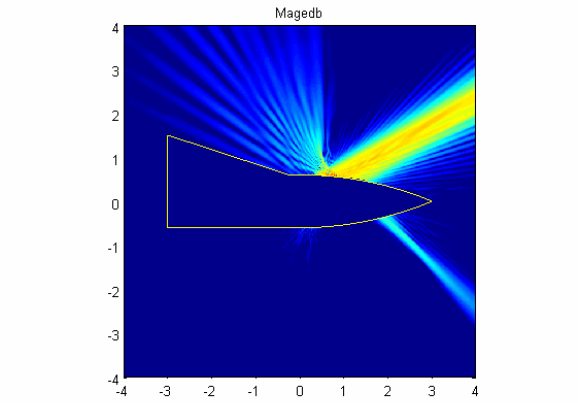

Figure 7: Fields outside cockpit.

Finally SPIKE can be used to calculate the reflected fields on surfaces inside the radome. Here the reflected fields are propagated back onto the antenna surface using the Kirchoff Huygen's principle. Figure 8 shows the reflected fields on the radome surface, whilst figure 9 shows the magnitude of the E fields on the antenna :

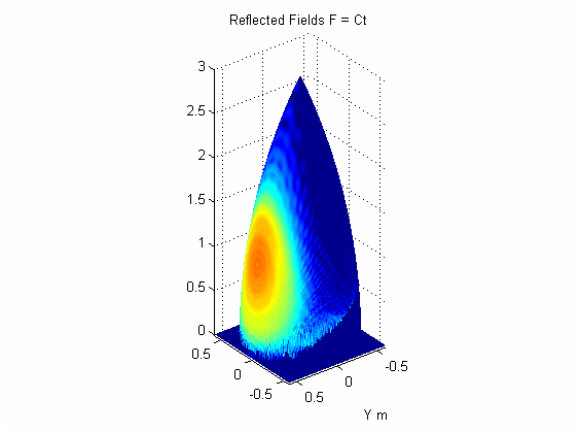

Figure 8: Reflected fields on radome surface

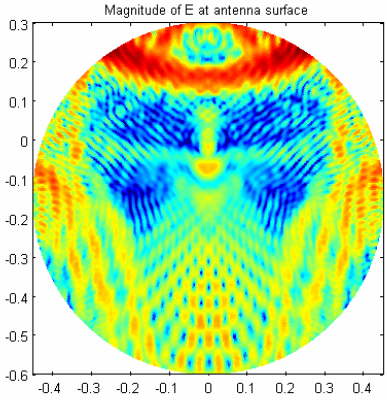

Figure 9: Reflected fields on antenna surface

The reflected power density on a given surface can be calculated from the **E** and **H** fields as follows:

$$P_{dens} = \frac{1}{2}\mathrm{Re}(\mathbf{E} \times \mathbf{H}^{*}) \quad (15)$$

6 Comparison of Results from SPIKE and GARD with flight trials data

GARD (Generic Airborne Radar Detection Model) is a radar model based on classical detection theory capable of simulating clutter maps while accounting for processing and atmospheric losses. It was used in conjunction with SPIKE antenna pattern data to provide a means of generating range-Doppler maps to compare with those produced by processing of flight trials IQ data obtained from an early experimental version of an e-scan radar system.

Figure 10 (a) shows an example of a range-Doppler map generated by GARD for an airborne platform at 6000 feet with a SPIKE generated antenna pattern and using a constant gamma land clutter model for an MPRF waveform. Figure 10 (b) shows a range-Doppler map for the same engagement scenario and radar parameters from a recorded flight trial with

the experimental radar system. The large clutter features near the main beam present in the GARD simulation show similarity to the features in the real data clutter plots. These are due to the flashlobes induced by the presence of the radome wall. The position and shape of the clutter was the main interest therefore no attempt was made to calibrate the amplitude characteristics of the model to account for the actual receiver AGC level. This explains the differences in noise levels between the simulated and real clutter plots. Comparative tests were performed at discrete beam pointing angles covering the full azimuth and elevation ranges for each PRF. It was found that the resulting GARD clutter maps accurately reproduced the gross clutter effects seen from the trials data thereby giving confidence that GARD in conjunction with SPIKE can capture the essential features of flight trials data.

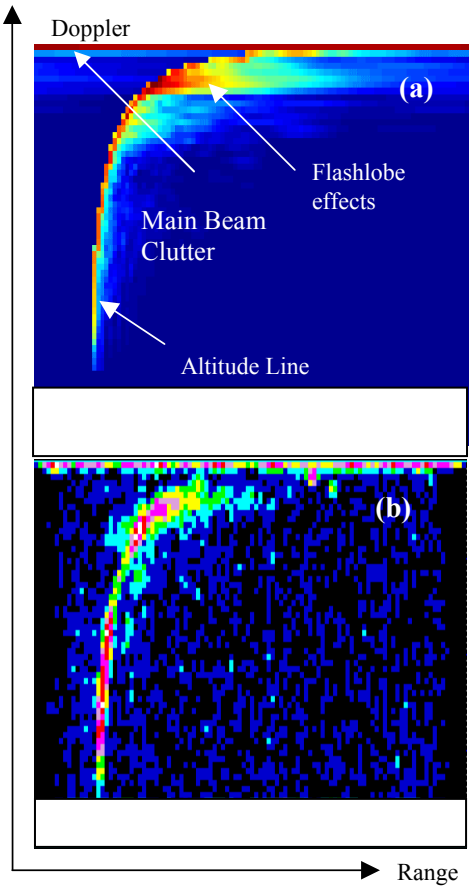

Figure 10: Comparison of SPIKE/GARD with flght trials data.

7 Summary and Conclusion

A new physical optics code SPIKE has been presented It shows greater flexibility than traditional ray tracing approaches in terms of the problems it can solve. Applications to predict second flashlobes and the near fields of antennas in various circumstances were presented. It has also been shown that SPIKE in conjunction with a radar detection model GARD can capture the essential features of flight trials data.

Acknowledgements

The authors wish to thank the management within SELEX S&AS for donating the time required to prepare and review this paper. Also Mr A Chalmers of SELEX S&AS design team for performing the GARD runs.

References

[1] Band C., Finlay C. Kinghorn A, Lyon R., Smith M 'Impact of radomes on airborne pulse Doppler radar performance.' Radar 2002 EICC 15-17 October 2002.
[2] Hecht E 'Optics' 3rd Edition Adison Wesley 1998 p 485
[3] Silver S, "Microwave Antenna Theory and Design", First Edition 1947, McGraw Book Company Inc., p 86.

Authors

Mr C. D. Finlay, Dr S. Gregson, Dr R. W. Lyon, Dr J. McCormick.